CrystEngComm

Accepted Manuscript

ROYAL SOCIETY OF CHEMISTRY

www.rsc.org/crystengcomm

Journal Name

ARTICLE

Synthesis of $ZnWO_4/CdWO_4$ core-shell structured nanorods formed by oriented attachment mechanism with enhanced photocatalytic performances

Received 00th January 20xx,
Accepted 00th January 20xx

DOI: 10.1039/x0xx00000x

www.rsc.org/

Di Li,*[a] Juanqin Xue[a] and Xiaojuan Bai[b]

$ZnWO_4/CdWO_4$ core-shell structured nanorods had been synthesized by a simple refluxing method under mild conditions in which the crystallization event of $ZnWO_4$ happened on the backbone of $CdWO_4$ single crystalline nanorods in a ligand-free system. $CdWO_4$ nanorod-directed oriented attachment mechanism had been clearly observed for the formation of $ZnWO_4/CdWO_4$ core-shell structured nanorods. The size of $ZnWO_4$ could be tuned by changing the molar ratio of Zn source and Cd source. The photocatalytic activity of $ZnWO_4/CdWO_4$ core-shell structured nanorods was much better than $CdWO_4$. The enhancement in photocatalysis performance was demonstrated to be the match of lattice and energy level between the $ZnWO_4$ and $CdWO_4$. This match facilitated the separation and transfer of photogenerated e^-/h^+ pairs at the heterojunction interfaces and might be important for other heterostructured materials. Kinetic studies using radical scavenger technologies suggested that photogenerated holes were the dominant photooxidants.

1. Introduction

The growth mechanism involving mostly oriented particle aggregation,[1-4] which was termed conceptually as 'oriented attachment' by Penn and Banfield et al.,[5-9] had emerged as highlighted by Alivisatos.[10] In this mechanism, the bigger particles are grown from small primary nanoparticles through an orientated attachment process, in which the adjacent nanoparticles are self-assembled by sharing a common crystallographic orientation and docking of these particles at a planar interface.[6]

Metal tungstates and molybdates, as a family of multicomponent metal oxide compounds, had been studied extensively due to their interesting structures, intriguing physical–chemical properties, as well as a wide range of applications in photoluminescence,[11] magnetic materials,[12] electrochemistry[13] and photocatalysis.[14–20] The $ZnWO_4$ and $CdWO_4$ represented a potential highly efficient photocatalytic material.[21–28] Therefore, there was a need to investigate the photocatalytic activity of the $ZnWO_4/CdWO_4$ core-shell structured photocatalyst.

In this paper, we described the oriented attachment mechanism in which the $CdWO_4$ nanorods obviously act as an epitaxial 'substrate' and guide the $ZnWO_4$ aggregation process for the formation of $CdWO_4$ nanorods based aggregated structures. The hierarchical $ZnWO_4/CdWO_4$ core-shell structured nanorods were controllably synthesized using a facile refluxing method under mild conditions. $CdWO_4$ nanorods form the backbone material, and the $ZnWO_4$ size could be tuned by changing the molar ratio of Zn source and Cd source. In addition, the photocatalytic activity and degradation mechanism of $ZnWO_4/CdWO_4$ core-shell structured nanorods in the degradation of methylene blue (MB) under ultraviolet light irradiation were investigated in detail.

2. Experimental section

2.1. Preparation of $CdWO_4$ nanorods and $ZnWO_4/CdWO_4$ core-shell structured nanorods

$CdWO_4$ nanorods were synthesized in a 50 mL capacity Teflon-lined stainless steel autoclave, which was done in a digital type temperature controlled oven. The detailed synthetic procedures of $CdWO_4$ nanorods had been described previously.[28] The synthesis of hierarchical $ZnWO_4/CdWO_4$ core-shell structured nanorods was performed in a flask with mild magnetic stirring for different periods. Typically, $CdWO_4$ nanorods were dispersed in 100 mL water. Then, $Zn(NO_3)_2$ and the same amount of Na_2WO_4 were added to the mother solution discontinuously. The solution was refluxed for 24h. Finally, the precipitate was washed by distilled water three times and dried for further characterization. The $ZnWO_4$ size could be tuned by changing the molar ratio of Zn source and Cd source.

2.2. Characterizations

X-ray diffraction (XRD) experiments were carried out using a Rigaku D/MAX–2500 diffractometer with Cu Ka radiation. The pH value was measured by OHAUS STARTER 2100/3C Pro-B pH meter. The size and morphologies of $CdWO_4$ and

[a]School of Metallurgical Engineering, Xi'an University of Architecture and Technology, Xi'an, 710055, China E-mail: lidi80315@gmail.com
[b]Academy of State Administration of Grain P.R.C, No. 11 Baiwanzhuang Avenue, Xicheng District, Beijing 100037, China

$ZnWO_4/CdWO_4$ core-shell structured nanorods were characterized by the aid of a JEOL JEM–2100F transmission electron microscope (TEM) and FEI Tecnai G2 F20 field transmitance electron microscope. The room temperature photoluminescence (PL) spectra of samples were investigated utilizing the Hitachi F-7000 Fluorescence Spectrophotometer. X-ray photoelectron spectroscopy (XPS) measurements were performed with Kratos AXIS ULTRA DLD. The transient photoluminescence measurements were carried out using a steady state and time-resolved fluorescence/phosphorescence spectrometer (FLSP920, Edinburgh Instruments Ltd.). EPR measurements of radicals spin-trapped by spin-trap reagent 5,50-dimethyl-1-pirroline-N-oxide (DMPO) (purchased from Sigma Chemical Co.) were carried out at room temperature with a JEOL ES-ED3X spectrometer equipped with a high-pressure mercury lamp as the irradiation source. To minimize experimental errors, the same type of quartz capillary tube was used for all EPR measurements. The EPR spectrometer was coupled to a computer for data acquisition and instrument control. Magnetic parameters of the radicals detected were obtained from direct measurements of magnetic field and microwave frequency.

2.3. Photocatalytic oxidative degradation

The photocatalytic activities of the $CdWO_4$ and $ZnWO_4/CdWO_4$ core-shell structured nanorods were evaluated by the MB decomposition under ultraviolet irradiation. Ultraviolet (UV) light was obtained by a 15 W Hg lamp (λ= 254 nm, Cnlight, Feshan) and the average light intensity was 600 μW cm^{-2}. The radiant flux was measured with a power meter (Beijing Normal University, Beijing). The photocatalytic degradation of MB in the aqueous solutions was studied by using $CdWO_4$ or $ZnWO_4/CdWO_4$ core-shell structured nanorods as the photocatalyst under room temperature and normal atmosphere pressure. $CdWO_4$ (50 mg) or $ZnWO_4/CdWO_4$ core-shell structured nanorods (50 mg) and 100 mL MB (2×10^{-5} M) aqueous solution were added into the reactor, and then stirred with a magnetic stirrer prior to irradiation with Hg lamp at room temperature. After the reaction, the sample solution was put in centrifuge to remove $CdWO_4$ particles from solution. The solution obtained this way was extracted into a quartz cell. The absorbance of the solution was measured with quartz cells every 5 min.

3. Results and discussion

3.1. Characterization of $ZnWO_4/CdWO_4$ core-shell structured nanorods

To determine the phase structures of the products, the X-ray diffraction (XRD) measurements were conducted. The backbone material $CdWO_4$ nanorods ($CdWO_4$: JCPDS card No. 87-1114) were identified by the XRD pattern shown in Fig. 1a. Because $CdWO_4$ (No. 87-1114: a = 5.029 Å, b = 5.86 Å, c = 5.071 Å, α=90°, β=91.5°, γ=90°) had a similar crystal lattice parameter as $ZnWO_4$ (No.88-0251: a = 4.693 Å, b = 5.721 Å, c = 4.928 Å, α=90°, β=90.63°, γ=90°), lattice matching between $CdWO_4$ and $ZnWO_4$ could exist.

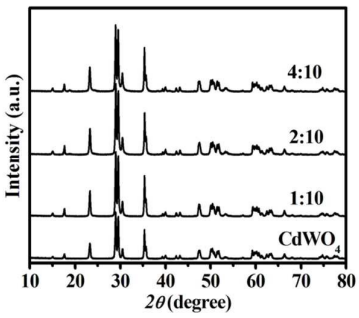

Fig. 1 XRD pattern of $CdWO_4$ nanorods and $ZnWO_4/CdWO_4$ core-shell structured nanorods.

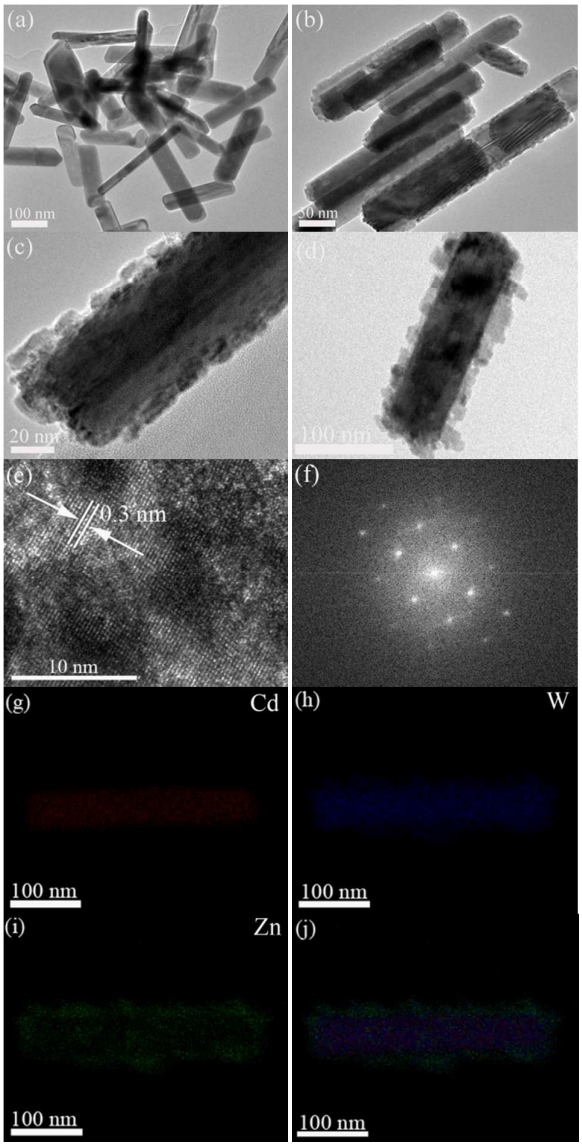

Fig. 2 (a) TEM images of $CdWO_4$ nanorods; (b)–(d) TEM images of the $ZnWO_4/CdWO_4$ core-shell structured nanorods obtained when the molar ratio of Cd source/Zn source in the reaction system was kept as 1:10, 2:10 and 4:10, respectively; HRTEM image of $ZnWO_4/CdWO_4$ core-shell structured nanorods:(e); the select area FFT pattern of $ZnWO_4/CdWO_4$ core-shell structured nanorods in (e); (g), (h) and (i) Cd, W and Zn elemental maps, respectively; (j) Cd, W and Zn elemental map together.

Fig. 2a–d showed the TEM images of the $CdWO_4$ nanorods and obtained $ZnWO_4/CdWO_4$ core-shell structured nanorods with different initial molar ratio of Zn source and Cd source. In Fig. 2a, pure $CdWO_4$ nanorods with the length of 150–200 nm and the diameter of 30–50 nm were used as the backbone material. The core-shell structure of the $ZnWO_4/CdWO_4$ sample were shown in Fig. 2b–d. Fig. 2b indicated that $ZnWO_4$ tend to attach on the backbone of the $CdWO_4$ nanorods. As shown in Fig. 2b–d, the size of $ZnWO_4$ would increase with increasing the molar ratio of Zn source and Cd source. When the molar ratio of Zn source and Cd source was 1:10, most of the as-obtained nanorods are of smooth surface (Fig. 2b). However, when the molar ratio increased from 1:10 to 2:10, 4:10, respectively, the surfaces of these nanorods became rougher and rougher (Fig. 2c and 2d), indicating that the size of $ZnWO_4$ shell became thicker. The microstructures of $ZnWO_4/CdWO_4$ core-shell structured nanorods were then investigated with high-resolution TEM (HRTEM). The HRTEM image (Fig. 2e) shows the interplanar spacing of the nanoflake was about 3.8 Å, which coordinates with the XRD peak for the [111] plane (2ϑ = 29.559°). The select area fast fourier transform (FFT) pattern as shown in Fig. 2f confirmed that the nanorods were single crystalline. In order to further confirm the chemical composition and elemental distribution, scanning transmission electron microscope (STEM) studies were performed. As displayed in Fig. 2g–j, the Cd, W and Zn elements were distributed in this nanorod. The Cd atoms were distributed in the 'core' of the nanorods; the Zn atoms were distributed at the surface of nanorods (Fig. 2i); whereas the W atoms spread all over the nanorods, indicating that the $ZnWO_4$ grown on the surface were mainly made of $ZnWO_4$ and the core-shell structures were a mixture of $ZnWO_4$ and $CdWO_4$, which agrees well with the results of XRD analysis.

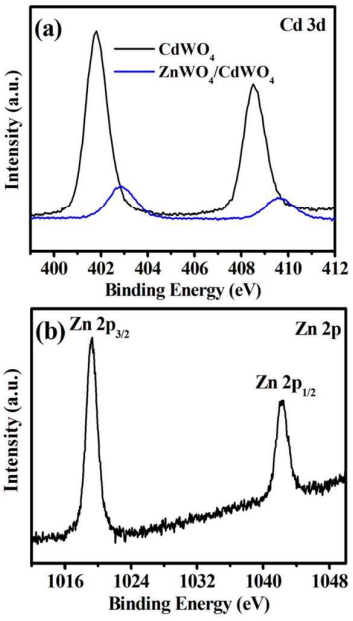

Fig. 3 XPS spectra for: (a) Cd 3d peak of pure $CdWO_4$ and $ZnWO_4/CdWO_4$ core-shell structured nanorods, (b) Zn 2p peak of $ZnWO_4/CdWO_4$ core-shell structured nanorods.

XPS was used to analyze the oxidation state and to further study the interaction of $CdWO_4$ covered with the $ZnWO_4$. The XPS spectra of Cd 3d for pure $CdWO_4$ and $ZnWO_4/CdWO_4$ (the molar ratio of Zn source and Cd source was 2:10), as well as the Zn 2p spectra for $ZnWO_4/CdWO_4$ were shown in Fig. 3a and 3b. The binding energy of Cd 3d of $ZnWO_4/CdWO_4$ exhibited an obvious shift as compared to pure $CdWO_4$ (Fig. 3a). These results showed that there was an intense interface interaction between Cd and $ZnWO_4$, not a simply physical adsorption. This interaction was essential to transfer carriers and enhance photocatalytic activity. The peak with binding energy for Zn 2p was detectable (Fig. 3b), indicating the existence of $ZnWO_4$, which was in good agreement with the results by the map analysis.

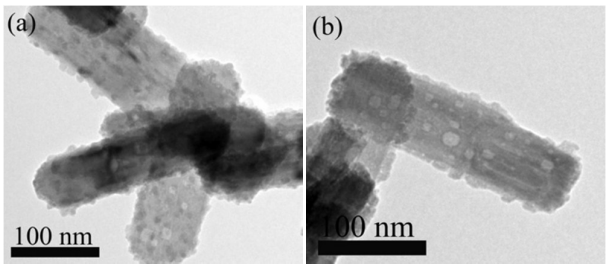

Fig. 4 Typical TEM images of the samples which were taken out after adding $Zn(NO_3)_2$ and Na_2WO_4 to a 100 mL solution containing 3 mmol $CdWO_4$ nanorods and refluxing the mixture for different period when the molar ratio of Cd source/Zn source in the reaction system was kept as 2:10: (a) refluxing for 6 h and (b) refluxing for 18 h.

3.2. Formation process of $ZnWO_4/CdWO_4$ core-shell structured nanorods

Refluxing of a fresh mixture of $Zn(NO_3)_2$ and Na_2WO_4 solutions in the presence of a suitable amount of single-crystal $CdWO_4$ nanorods at for different reaction times produced $ZnWO_4/CdWO_4$ core-shell structured nanorods with typical shapes as shown in Fig. 4a and 4b. Fig. 4a indicated that $ZnWO_4$ tend to attach on the backbone of the $CdWO_4$ nanorods. As the reaction continued, the $ZnWO_4$ grew (Fig. 4b).

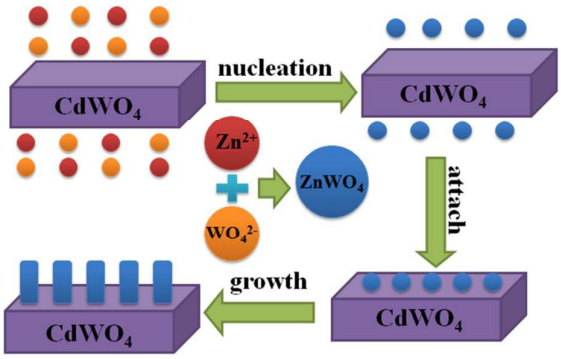

Scheme 1 Schematic drawing illustrating the formation process of the $ZnWO_4/CdWO_4$ core-shell structured nanorods.

3.3. $ZnWO_4/CdWO_4$ core-shell structured nanorods growth mechanism

The growth mechanism of 'oriented attachment' was proposed to demonstrate the complicated nano-architecture

process. The oriented attachment mechanism described the spontaneous self-organization of adjacent particles, so that they shared a common crystallographic orientation, followed by the joining of these particles at a planar interface.[13] The process was particularly relevant in the nanocrystalline regime, where bonding between the particles reduces overall energy by removing surface energy associated with unsatisfied bonds.[29] In the reaction, $CdWO_4$ nanowrods were used as the 'substrate', which can guide the $ZnWO_4$ self-assembling growth in aqueous solution without surfactant and stabilizers. Then the 'oriented attachment' could guide the $ZnWO_4$ oriented growth. As shown in Scheme 1, supersaturated solution with plenty of $ZnWO_4$ small crystals were formed by adding Zn resource. Because of the high surface energy and thermodynamics instability, $ZnWO_4$ could attach to the surface of $CdWO_4$ to decrease surface energy. The crystallographic orientation of the particles with respect to each other was determined by the minimization of the highest surface energy. Therefore, with a matching lattice, the lattice fringes' orientation and crystal growth direction were uniform to some extent. The 'substrate', $CdWO_4$, had similar lattice parameters and could control $ZnWO_4$ to form $ZnWO_4/CdWO_4$ core-shell structured nanorods.

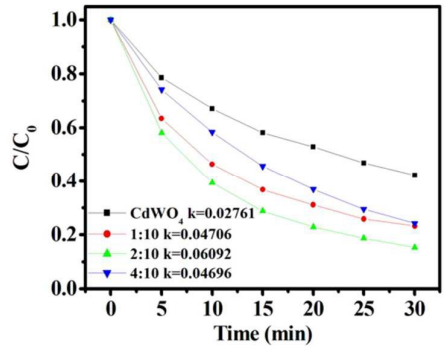

Fig. 5 First-order plots for the photocatalytic degradation of MB using $CdWO_4$ nanorods and $ZnWO_4/CdWO_4$ core-shell structured nanorods.

3.4. Photocatalytic properties of $ZnWO_4/CdWO_4$ core-shell structured nanorods

The photoactivity of $ZnWO_4/CdWO_4$ core-shell structured nanorods were evaluated by degradation of methylene blue (MB), a hazardous dye as well as a common model to test the photodegradation capability.[30-32] To further depict the photocatalytic reaction, the photocatalytic degradation process was also fitted to pseudo-first-order kinetics, and the value of the rate constant k was equal to the corresponding slope of the fitting line, as shown in Fig. 5. The first-order linear relationship was revealed by the plots of the $\ln(C/C_0)$ vs irradiation time (t), where C was the concentration of MB at the irradiation time t and C_0 was the concentration in the adsorption equilibrium of the photocatalysts before irradiation. Via the first order linear fit, the determined reaction-rate constants k were 0.02761, 0.04706, 0.06092 and 0.04696 min^{-1}, respectively, for $CdWO_4$ nanorods and $ZnWO_4/CdWO_4$ core-shell structured nanorods with different molar ratio of Zn source and Cd source from 1:10 to 4:10. The photocatalytic rate constant was obvioudly enhanced with increasing the $ZnWO_4$ content. When molar ratio of Zn source and Cd source was 2:10 (ZC-2), it exhibited the highest photocatalytic activity. The apparent rate constant k was 0.06092 min^{-1}, which was more than twice as high as $CdWO_4$ nanorods. However, as the proportion of $ZnWO_4$ further increases, the degradation rate decreases gradually though it remained higher than that of $CdWO_4$. This change in UV activity of $ZnWO_4/CdWO_4$ core-shell structured nanorods samples might be attributed to the excitation of $CdWO_4$. Although $ZnWO_4$ were beneficial for charge transfer at heterojunction interfaces, they would shield UV light off of $CdWO_4$. Therefore, due to the demands of both the charge transfer and light harvesting, our photocatalytic activity first increased and then decreased with the increasing amount of $ZnWO_4$, which resulted in the best photocatalytic activity of ZC-2. Additionally, the surface area of $CdWO_4$ nanorods and $ZnWO_4/CdWO_4$ core-shell structured nanorods were similar (Table 1), so the surface area had no effort on photocatalysis activity.

Table 1 The BET results of $CdWO_4$ nanorods and $ZnWO_4/CdWO_4$ core-shell structured nanorods.

sample	$CdWO_4$	1:10	2:10	4:10
BET surface area ($m^2\ g^{-1}$)	10.3789	8.2022	9.5981	14.5013

It was important to detect the main oxidative species in the photocatalytic process for revealing the photocatalytic mechanism. The main oxidative species in the photocatalytic process could be detected through the trapping experiments of radicals and holes by using tert-butanol (hydroxyl radical scavenger)[33,34] and citric acid (hole scavenger),[35] respectively. As shown in Fig. 6, the addition of a scavenger of radicals (tert-butanol) only caused a smaller change in the photodegradation of MB, indicating that the free hydroxyl radicals was not the main active oxygen species in the photocatalytic process. On the contrary, the photocatalytic activity of $ZnWO_4/CdWO_4$ could be greatly suppressed by the addition of a scavenger for holes (citric acid). This result suggested that the photogenerated holes were the main oxidative species of the $ZnWO_4/CdWO_4$ system.

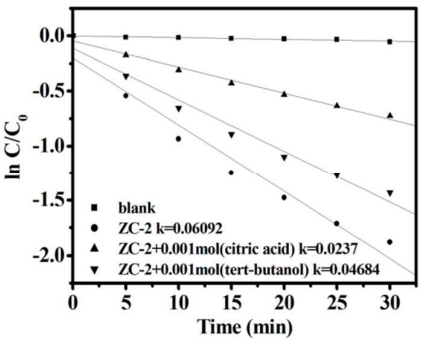

Fig. 6 Effects of tert-butyl alcohol and citric acid addition on photocatalytic degradation of MB in solutions of ZC-2.

Although photogenerated holes were the main oxidative species, the reaction-rate decreased more than one fourth after adding tert-butyl alcohol (hydroxyl radical scavenger). It meant hydroxyl radicals took a part in photooxidation of MB. EPR spectroscopy was an especially suitable technique for the detection of photogenerated radicals, which act as intermediates in the photocatalytic processes. Here ZC-2 nanorods in water were used to investigate the EPR signal at room temperature under the irradiation of a high-pressure mercury lamp. Results of the EPR signals from ZC-2 nanorods in water were shown in Fig. 7. No ESR signals were observed when the reaction was performed in the dark in the presence of the catalysts. Under UV irradiation, the characteristic peaks of the $O_2^{\bullet-}$ could be observed after 1 min illumination period. And the superoxide radical anion tends to converting to OH• with the irradiation time increasing.[36,37] The intensity of the OH• further increased with 3 min of irradiation.

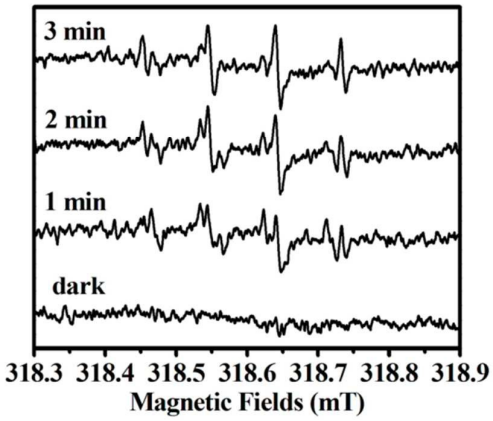

Fig. 7 EPR spectra of ZC-2 under UV light irradiation (DMPO as the radical trapper).

N-demethylation of MB was observed by Mohammad and Morrison[38] during "photodynamic therapy" studies using visible light irradiation (λ > 520 nm). N-dealkylation of dyes containing auxochromic alkylamine groups played an important role in photocatalytic degradation. The colour of MB solutions became less intense (hypsochromic effect) when all or part of the auxochromic groups (methyl or methylamine) degraded. Fig. 8 showed that the spectral band at 664 nm blue-shift during the course of the photodegradation. As weak electrondonor substituents, methyl groups could facilitate attack on MB by electrophilic species (OH• or hole) in the demethylation process; this was also likely to be a major step in the photocatalytic oxidative degradation of MB.[39] Examination of the spectral variations in Fig. 8 suggested that MB was N-demethylated in a stepwise manner (methyl groups were removed one at a time as confirmed by the gradual peak wavelength shifts toward the blue region), with cleavage of the MB chromophore ring structure occurring concomitantly. N-demethylation, deamination and oxidative degradation took place during the photocatalyzed degradation of MB.[39] Mixtures of N-demethylated intermediates yielded spectra with broad absorption bands in the visible range.

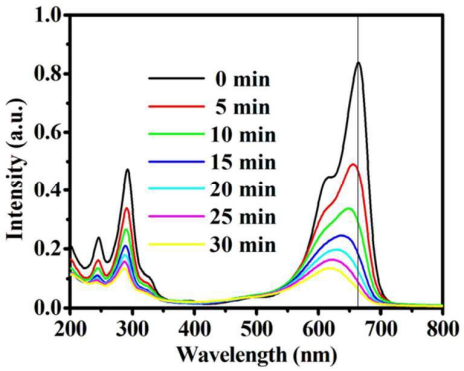

Fig. 8 The UV-vis spectral changes of MB (ZC-2: 0.5 g L^{-1}; MB: 2×10^{-5} M).

The above results showed that the coating of $ZnWO_4$ could enhance UV activity of $CdWO_4$. As was well known, this might be due to the high separation and transfer of photogenerated electron–hole pairs at the heterojunction interfaces. Fig. 9 gave time-resolved transient photoluminescence decays of $CdWO_4$ and sample ZC-2. The photoluminescence lifetime of $CdWO_4$ and $ZnWO_4$/$CdWO_4$ core-shell structured nanorods was on the order of nanoseconds, and the photoluminescence lifetime of ZC-2 was higher than $CdWO_4$: ZC-2 (28.19 ns) > $CdWO_4$ (11.34 ns). A longer photoluminescence lifetime meant lower recombination rate of the electron–hole pairs, and thus higher photocatalytic activity.[40]

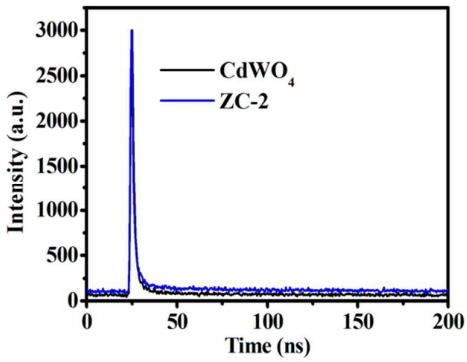

Fig. 9 Time-resolved transient photoluminescence decays of $CdWO_4$ and ZC-2.

This high separation efficiency may be due to the energy level match between $ZnWO_4$ and $CdWO_4$. Scheme 2 showed the schematic for e^-/h^+ separation and transportation at the $ZnWO_4$/$CdWO_4$ core-shell structured nanorods interface. Both $ZnWO_4$ and $CdWO_4$ can absorb UV light to produce photogenerated electron-hole pairs. Since the valence band (VB) position of $ZnWO_4$ (+2.9 eV) is higher than the VB of $CdWO_4$ (+3.43 eV),[41,42] the photogenerated holes on the VB of $CdWO_4$ can directly transfer to the VB of $ZnWO_4$. On the contrary, conduction band (CB) position of $ZnWO_4$ (–0.8 eV) is higher than the CB of $CdWO_4$ (+0.13 eV). So the excited-state electrons from the CB of $ZnWO_4$ started to diffuse into the CB of $CdWO_4$. Therefore, an effective charge separation was achieved, resulting in an increased photocatalytic activity.

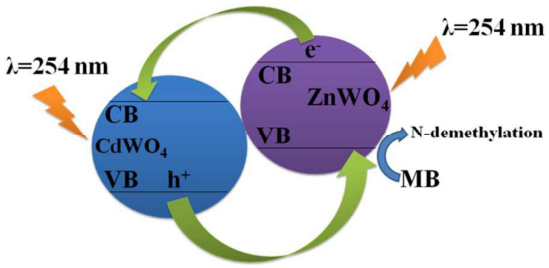

Scheme 2. Schematic drawing illustrating the mechanism of charge separation and photocatalytic activity over a $ZnWO_4/CdWO_4$ core-shell structured nanorods under ultraviolet light irradiation.

4. Conclusions

In summary, $ZnWO_4/CdWO_4$ core-shell structured nanorods could be synthesized by a facile refluxing method under mild conditions in which the crystallization event of $ZnWO_4$ occurred on the backbone of $CdWO_4$ nanorods. The size of $ZnWO_4$ could be tuned by changing the molar ratio of these raw materials. The enhancement of UV light performance was induced by the high separation efficiency of photoinduced electron–hole pairs. This high separation efficiency might be due to the heterojunction interfaces induced by the lattice and energy match. The $ZnWO_4/CdWO_4$ core-shell structured nanorods described in this paper might have potential applications in photocatalytic decomposition of MB.

Acknowledgements

This work was supported by Chinese National Science Foundation (21301135).

Notes and references

1 J. K. Bailey, C. J. Brinker and Mecartney, M. L. *J. Colloid Interface Sci.*, 1993, **157**, 1.
2 M. Ocaña, M. P. Morales and C. J. Serna, *J. Colloid Interface Sci.*, 1995, **171**, 85.
3 V. Privman, D. V. Goia, J. Park and E. Matijević, *J. Colloid Interface Sci.*, 1999, **213**, 36.
4 A. Chemseddine and T. Moritz, *Eur. J. Inorg. Chem.*, 1999, 235.
5 R. Lee Penn and J. F. Banfield, *Geochim. Cosmochim. Acta*, 1999, **63**, 1549.
6 R. Lee Penn and J. F. Banfield, *Science*, 1998, **281**, 969.
7 J. F. Banfield, S. A. Welch, H. Zhang, T. T. Ebert and R. Lee Penn, *Science*, 2000, **289**, 751.
8 R. Lee Penn, G. Oskam, T. J. Strathmann, P. C. Searson, A. T. Stone and D. R. Veblen, *J. Phys. Chem. B*, 2001, **105**, 2177.
9 R. L. Penn, A. T. Stone and D. R. Veblen, *J. Phys. Chem. B*, 2001, **105**, 4690.
10 A. P. Alivisatos, *Science*, 2000, **289**, 736.
11 B. Liu, S.-H. Yu, L. Li, F. Zhang, Q. Zhang, M. Yoshimura and P. Shen *J. Phys. Chem. B*, 2004, **108**, 2788.
12 Q. Zhang, X. Chen, Y. Zhou, G. Zhang and S.-H. Yu, *J. Phys. Chem. C*, 2007, **111**, 3927.
13 L. Mai, F. Yang, Y. Zhao, X. Xu, L. Xu and Y. Luo, *Nat. Commun.*, 2011, **2**, 381.
14 L. Zhou, W. Wang, H. Xu and S. Sun, *Cryst. Growth Des.*, 2008, **8**, 3595.
15 S. Song, Y. Zhang, Y. Xing, C. Wang, J. Feng, W. Shi, G. Zheng and H. Zhang, *Adv. Funct. Mater.*, 2008, **18**, 2328.
16 D. Li and Y. Zhu, *CrystEngComm*, 2012, **14**, 1128.
17 F. Amano, A. Yamakata, K. Nogami, M. Osawa and B. Ohtani, *J. Am. Chem. Soc.*, 2008, **130**, 17650.
18 M. Shang, W. Wang and H. Xu, *Cryst. Growth Des.*, 2009, **9**, 991.
19 X. Zhao and Y. Zhu, *Environ. Sci. Technol.*, 2006, **40**, 3367.
20 H. F, L. Zhang, W. Yao and Y. Zhu, Zhu, *Appl. Catal., B*, 2006, **66**, 100.
21 H. Fu, J. Lin, L. Zhang and Y. Zhu, *Appl. Catal., A*, 2006, **306**, 58.
22 G. Huang, C. Zhang and Y. Zhu, *J. Alloys Compd.*, 2007, **432**, 269.
23 J. Lin, J. Lin and Y. Zhu, *Inorg. Chem.*, 2007, **46**, 8372.
24 R. Shi, Y. Wang, D. Li, J. Xu and Y. Zhu, *Appl. Catal., B*, 2010, **100**, 173.
25 D. Li, R. Shi, C. Pan, Y. Zhu and H. Zhao, *CrystEngComm*, 2011, **13**, 4695.
26 D. Ye, D. Li, W. Zhang, M. Sun, Y. Hu, Y. Zhang and X. Fu, *J. Phys. Chem. C*, 2008, **112**, 17351.
27 W. Tong, L. Li, W. Hu, T. Yan and G. Li, *J. Phys. Chem. C*, 2010, **114**, 1512.
28 D. Li, X. Bai, J. Xu, X. Ma and Y. Zhu, *Phys. Chem. Chem. Phys.*, 2014, **16**, 212.
29 M. Niederberger and H. Cölfen, *Phys. Chem. Chem. Phys.*, 2006, **8**, 3271.
30 S. U. M. Khan, M. Al-Shahry and W. B. Ingler Jr., *Science*, 2002, **27**, 2243.
31 K. H. Ji, D. M. Jang, Y. J. Cho, Y. Myung, H. S. Kim, Y. Kim and J. Park, *J. Phys. Chem. C*, 2009, **113**, 19966.
32 L. Zhang, Y. Wang, H. Cheng, W. Yao and Y. Zhu, *Adv. Mater.*, 2009, **21**, 1286.
33 L. Zhang, H. Cheng, R. Zong and Y. Zhu, *J. Phys. Chem. C*, 2009, **113**, 2368.
34 S. Zhu, T. Xu, H. Fu, J. Zhao and Y. Zhu, *Environ. Sci. Technol.*, 2007, **41**, 6234.
35 K. Kabra, R. Chaudhary and R. L. Sawhney, *J. Hazard. Mater.*, 2008, **155**, 424.
36 H. Fu, C. Pan, W. Yao and Y. Zhu, *J. Phys. Chem. B*, 2005, **109**, 22432.
37 M. R. Hoffmann, S. T. Martin, W. Choi and D. W. Bahneman, *Chem. Rev.*, 1995, **95**, 69.
38 T. Mohammad and H. Morrison, *Photochem. Photobiol.*, 2000, **71**, 369.
39 T. Zhang, T. Oyama, A. Aoshima, H. Hidaka, J. Zhao and N. Serpone, *J. Photochem. Photobiol., A*, 2001, **140**, 163.
40 C. Pan, J. Xu, Y. Wang, D. Li and Y. Zhu, *Adv. Funct. Mater.*, 2012, **22**, 1518.
41 Y. Wang, Z. Wang, S. Muhammad and J. He, *CrystEngComm*, 2012, **14**, 5065.
42 I. Aslam, C. Cao, M. Tanveer, M. H. Faroog, W. S. Khan, M. Tahir, F. Idrees and S. Khalid, *RSC Adv.*, 2015, **5**, 6019.

We described the oriented attachment mechanism in which the $CdWO_4$ nanorods obviously act as an epitaxial 'substrate' and guide the $ZnWO_4$ aggregation process for the formation of $CdWO_4$ nanorods based aggregated structures.